Ali Hussein F Alnasraui /J. Pharm. Sci. & Res. Vol. 10(3), 2018, 442-449

ISSN:0975-1459
Journal of Pharmaceutical Sciences and Research
www.jpsr.pharmainfo.in

Development of SOI Based Microdosimeter for Tackling Tissue Equivalence by BNCT and Fast Neutron and Proton Therapy

Ali Hussein F Alnasraui
College of Biotechnology. Department of Biotechnology AlQasim Green University/Iraq

Abstract

In this paper a microdosimeter is constructed using silicon-on-insulator to define the sensitive volume depth and tissue equivalence under geometric scaling which includes the energy deposition spectrum. Microdosimetric quantities are described which includes frequency and dose distribution and based upon the requirement constraints a microdosimeter is designed by performing noise minimization. The experimental model is briefly presented with necessary circuit diagrams. The experiment embodies I-V and C-V testing along with a noise optimization approach. The collection efficiency and radiation hardness is characterised.

Keywords: Silicon-on-insulator, Tissue equivalence, I-V and C-V testing, Noise optimization, Collection efficiency.

1. INTRODUCTION

Microdosimeter is a compact device that directly calculates the radiation dose absorbed by a silicon device. Energy is absorbed from electrons, protons and gamma rays so that the total dose from other electronic devices gets absorbed. By the process of ionization and excitation, energy is deposited over the irradiated body in a non-uniform motion. It is measured as a standard quantity which specifies the average deposition per unit mass. These effects are also established by the microscopic spectrum relating to the sensitive matters of the irradiated body. Biological effects (biological effectiveness) differ with respect to the energy distribution, even-though the absorbed radiation dose is same. In [1] silicon based microdosimeter is reviewed and is compared with proportional gas counter. The implementation of microdosimeter did not meet the expectations since the requirements of shape, tissue equivalence, charge collection and noise factors hindered its development. However, silicon on insulator approach was performed using high LET radiotherapy which proved to be comparatively better than the proportional gas counter since the former method overcame the drawbacks such as effective simulation of array cells and reduction in physical size. [2] Some of the microdosimeter devices are equipped with a tissue equivalent proportional counter where a low pressured gaseous substance is used to simulate sensitive volume. Its tissue equivalency was found to be far better but results in a list of shortcomings like, wall effects and spatial resolution limitations.

Microdosimetry also involves in investigation of spatial, temporal and spectral aspects of microscopic energy deposition criteria. To analyse the ionizing radiation through various radiation effects, microdosimetric field enables the systematic study of quantification. In [3] silicon dosimeter was designed to respond with neutrons and hadron-therapy beams. Monolithic telescope technology was employed to minimize the filed-funnelling effect. The proposed method was opted for quality assessment of hadron-therapy rays and to determine neutron fields. The implementation of silicon telescope to measure microdosimetric spectra was not satisfactory since it was limited to minimal absorption range. In [4] construction of microdosimetry was presented using silicon-on-insulator detector. Microdosimeter studies revealed that SOI detectors record the energy deposition at various radiation fields. The paper also includes an alternative mechanism to this which is named to be monolithic ΔE-E silicon telescope. The basic requirements to design a silicon based microdosimeter is briefly explained and according to it, the design is structured. While most of the literature works convey its applications to radiobiology, it is also necessary to focus on its application over the radiation effects, radiobiology, radiotherapy and radio-protection over electronics where the pattern of energy deposition is measured in small sized volumes since the measurements are scaled at micron levels. A low pressure proportional counter had been used so far as a primary device for such lower range measurements. Though it can be regarded as a suitable detector its drawbacks are more. Certain shortcomings can be listed as follows,

- Larger physical size
- Lower spatial resolution
- Inability to simulate array of cells
- Pileup, phase and wall effect errors

Silicon based microdosimetry deals with smaller size, it is worth-able for its spatial resolution due to the advanced development phase of the integrated circuit technology. While the demerits in electronics are solved using microdosimetry, it also impedes a lot of problems such as tissue equivalence, sensitive volume and noise defects in medical applications. [5] Microdosimetric measurements using tissue equivalent proportional counter was described to identify microdosimetric spectra. Ionizing particles were produced by developing a composite made of nitrogen, boron, lithium or cadmium. It suggested that this method is suitable only for internal dosimetry applications. [6] Application of micro-dosimetric spectrum in microelectronics was emphasised by reviewing the radiation effects. The basic distributions that influence the ionizing fluctuations were illustrated on the basis of Poisson process theory. Dose fluctuations were analytically elaborated for both the terms of ionic and electronic events. Threshold dose is assessed with extreme value and microdosimetric theory. The experimental data based on silicon proportional counter was included. Though efficient results were obtained, the processing was found to be complicated in implementing the values to the corresponding application sectors. [7, 8] Microdosimeter based on cylindrical diodes and solid state detectors are presented using 3D micro-fabrication technology. The biophysical factors to attain hadron therapy effectiveness were developed. The requirements in adapting an accurate size of micro sensor is complex and the analytical solutions for the charge limited current could have been more effective. [9] Development of 3D bridge microdosimeter to define charge collection for radiation therapy was described. The limitations of conventional tissue equivalent proportional counter including the requirement of high voltage of operation and large size device were mentioned and such shortcomings were reduced by the proposed technique. Still, the problem occurs due to its complex networking structures and maintenance difficulties. [10, 11, 12] Microdosimetric detectors provide high spatial and energy resolution. Some of the defects were identified as noise characterization, radiation hardness, sensitive volume, non-tissue

equivalence and field funnelling effect. The feasibility studies of all these limitations are elaborated using monolithic silicon telescope, 2-stage detectors and mono-energetic neutrons and the corrections of a few of the drawbacks are suggested. SOI technology in experimental microdosimetry provides high spatial resolution and count rates. The objective of the research is to investigate the problems such as tissue equivalence, noise minimization, sensitive volume structure and shape of the device confronting silicon microdosimetry and to develop a highly efficient device by getting rid of all the above mentioned difficulties. The feasibility of the presented microdosimetric design in high lineal energy transfer fields is validated by a set of tests at conditions of boron neutron capture and fast neutron therapy.

Since most of the referred articles end in results of negative impacts, this approach is relatively better concerning noise minimization and effective processing. Considering all the factors such as tissue equivalence, requirement of area, size and shapes of materials used and drawbacks of the traditional and existing systems, the research is done with utmost care in bringing out the most productive results in the field of both internal and external microdosimetric sectors.

2. METHODOLOGIES

2.1. Microdosimetric quantities

The lineal energy spectrum of the rectangular parallelepiped silicon microdosimeter closely resembles the spherical structure. Lineal energy is the prime concept which is defined by,

$$y = \frac{\varepsilon}{\bar{l}}\ keV\mu m^{-1} \qquad (2.1)$$

$$\bar{l} = \frac{4V}{S} \qquad (2.2)$$

where, y is the lineal energy, ε is the energy, $\bar{l}$ is the mean length of chord, V is the volume and S is the surface area. y is related to fluctuations of the delta ray effects of LET and chord length variations.

The probability function of y is the basic parameter of microdosimetry. The relation between probability distribution f(x) and dose distribution, d(x) is,

$$d(y) = \frac{yf(y)}{\bar{y}_F} \qquad (2.3)$$

$$f(y) = \exp(-y);\ \bar{y}_f = 1 \qquad (2.4)$$

y is exponentially distributed and hence

$$\bar{y}_F = \int_0^\infty yf(y)dy \qquad (2.5)$$

Linear energy can be considered either as a frequency distribution or as a dose-wise distribution. Frequency distribution is shown in table 1 and the corresponding graphical representation is plotted in figure 1.

Table 1.Frequency distribution

y	f(y)
0.0	0.986486
1.25	0.788712
2.34	0.641815
2.55	0.379413
3.57	0.148545
3.63	0.122524
4.57	0.070637
6.37	0.004615
7.61	0.004914
8.24	0.00704
9.28	0.017408

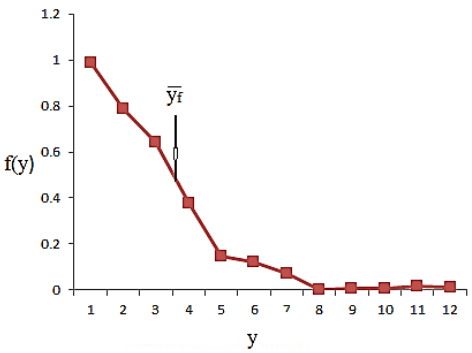

Figure 1.Frequency distribution

The tabulation (table 2) and the graphical representation (figure 2) of dose distribution are as follows:

Table 2.Dose distribution

y	d(y)
0.0	0.004459
0.52	0.209554
0.58	0.251911
0.93	0.327707
1.12	0.341083
1.64	0.316561
2.24	0.263057
2.61	0.191725
3.48	0.113694
3.75	0.086943
4.32	0.046815
5.42	0.026752
6.05	0.015605
8.14	0.006688
10.6	0.008917

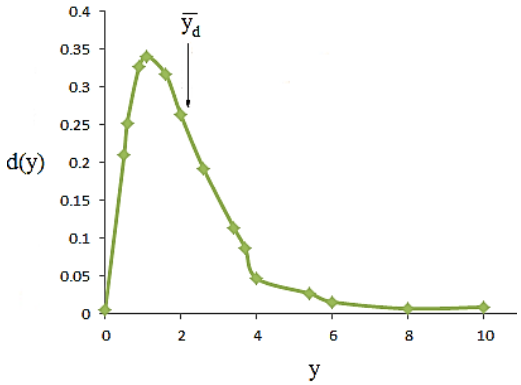

Figure 2.Dose distribution

$$d(y) = \frac{y}{\bar{y}_F} f(y) \qquad (2.6)$$

$$\bar{y}_D = \int_0^\infty yd(y)dy \qquad (2.7)$$

$$\bar{y}_D = \frac{1}{\bar{y}_F}\int_0^\infty y^2 f(y)dy \qquad (2.8)$$

Microdosimetric distributions can be determined by lineal energy distribution and site geometry. It can be denoted as a log-linear plot with the function multiplied by y. This function is given as yf(y) and yd(y),

$$\int d(y)dy = \int yd(y)d(\ln(y)) = \ln(10)\int yd\,(y)d(\log y) \qquad (2.9)$$

2.2. Requirements of a microdosimeter

The requirements of microdosimeter depend upon the applications in which they are intended to be used. For certain list of applications, use of silicon detectors would not be helpful, i.e. the interaction of radiation and the secondary charged particles in silicon and tissue volume varies. Silicon devices are suitable for use in radiation medium. The components are insider, stopper, crosser and starter. Stopper starts from outside the tissue volume and ends within it, starter and crosser begins from and outside the tissue and goes beyond it respectively where insider retains within the tissue volume. Most of the events should be crossers or stoppers which are initiated by the converter at the apex of the detector. Secondary particles extending the detector volume differs with respect to the applications. The radiation dose is calculated by the microdosimetric spectra. The process includes several uncertainties which reduce the measurement accuracy. However certain uncertainties are acceptable but a range of more than 30% is not permitted.

Proton therapy and fast and boron neutron capture therapy are the high LET radiation modes described in this work. Errors are calculated and compared to find out the fluctuations in regional microdosimetry. Random processes influence the shape of the pulse height distribution where relative variance is used to quantify the results which is expressed as,

$$V = \frac{\sigma^2}{m_1^2} = \frac{m_2}{m_1^2} - 1 \qquad (2.10)$$

where V is the relative variance, σ^2 is the variance and m_1&m_2 are the moments of f(x)

2.2.1. Detector models

Energy deposition of microdosimetry should be modelled in equivalence with the biological cell structures. Generally, spherical components are preferred to cylindrical designs. The main reasons behind the usage of spherical shape are its isotropic response and lower relative variance. Planar lithographic technology is employed in the integration of circuit processing. The project is comprised of different shapes of chord and segment distributions along with rectangular, cylindrical and hemispherical shapes. Thus by analysing and comparing several shapes, ideal design for silicon microdosimeter is generated.

The Chord Length Distribution (CLD) is determined for each shape to compare the microdosimetric spectrum. CLD occurs due to the intersection of convex structure with random straight lines and as a result, μ, ν and λ randomness are produced. Among these, μ-randomness is widely used as it is similar to microdosimetric experiments.

Segment Length Distributions (SLD) are analysed as before, where the randomness conditions of SLD resembles CLD with the addition of finite range rays. The effect of finite rays is considered when the detector relies over the converter which is above the silicon volume.

CLD and SLD are employed to compare microdosimetric spectra of different shapes. To compare the performance of shapes, mean energy imparted per event, $\overline{\varepsilon_d}$ is determined. $\overline{\varepsilon_d}$ can be calculated by CLD or using proximity function. Proximity function is defined by the measurement of probability distribution. $\overline{\varepsilon_d}$ for a uniform isotropic radiation field is given as,

$$\overline{\varepsilon_d} = \int_0^{x_{max}} \frac{s(x)t(x)}{4\pi x^2} dx \qquad (2.11)$$

$$\overline{\varepsilon_d} = \int_0^{x_{max}} U(x)t(x)dx \qquad (2.12)$$

where (x) is the geometric reduction factor, s(x) is the integral proximity function, t(x) is the proximity function and x is the shell radius.

Proximity function is favoured over chord length distribution due to its simplicity. Detector volumes are chosen to reduce the relative variance. To tackle this spherical structure would be enough since it has the minimal relative variance. The thickness of the over-layer and the detector must be minimum. Cubical length of 0.837d is equal to the spherical diameter. Shape and tissue equivalence corrections are determined to analyse the dimensions of silicon detector.

2.2.2. Geometrical and operational requirements

Normally, detector dimensions are calculated on the basis of detector size since the device size should be equivalent to the biological entity under study so that the radiobiological data of the microdosimetric spectrum would be maximised. The dimension of silicon microdosimeter would be better if it ranges around 13μm where the radiobiological site size of 2μm is acceptable. Its cross sectional area varies with respect to the flux of the radiation field. Proportional counters with diameters around 20cm would be favourable. An array of sensitive volumes is used by the detector to enhance the collection techniques. Complexity charge collection should be kept reduced in funnelling effects and particularly with diffusion. Radiobiological effectiveness is directly proportional to lineal energy which rises beyond unity if the lineal energy goes above ~1keV. To obtain the spectrum in every radiation fields, lineal energy of less than 1keV is applicable, but for most of the microdosimetric measurements, the value should be equal or more than that of 1keV

3. Design Of Microdosimeter

As-how the requirements are stated, silicon dosimeter is designed using existing detectors, components and memory cell arrays. Each cell of RAM consists of around six transistors. In a memory system, reverse biased junction of high electric field is sensitive to radiation. Its state varies from 0 to 1 or vice-versa when charge gets collected from sensitive areas which is said to be bit-flip. A comparison is made among memory and living cells where both are quite similar in the view of microdosimetry. So, failure of RAM is comparable to cell death. The so called demerits of RAM are charge collection and volume boundaries. Charge collection which depends on number of diode junctions, electric fields, drift and diffusion effects is complex and the boundaries are sensitive. Charge collections must be simple inorder to verify the simulation modelling which could be performed by a bit-flip or single event upset test instrument. This can be applied to medical systems as well.

3.1. Experimental design

The test units of silicon microdosimeter consist of SOI wafers with varying thickness. Generally charge collection is done by a reverse biased p-n junction diode and this process gets complicated due to the additional charge collection by diffusion. Charge collection from the lower end of the SOI layer can be prevented by SOI structures due to the presence of an insulated layer under it. This is one of the advantages of using SOI. The representation (figure 3) based on scanning electron microscope over SOI construction is shown as,

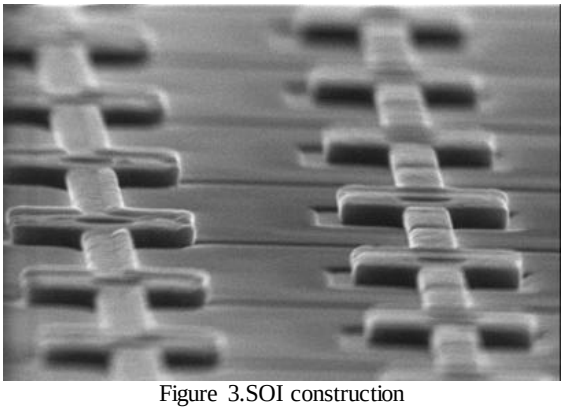

Figure 3.SOI construction

3.2. Electrical specifications

I-V values are calculated to test the integrity of the diode and to determine noisy factors. For this purpose, a unit named, Keithley 237 HV is used which is controlled by metrics software. The readings are defined as:

- Reverse bias measurement: -10-0V (0.1 volt steps)
- Forward bias measurement: 0-0.45V (0.05 volt steps)
- Current value: <100µA
- Settling time: 3 sec
- Temperature: 22-28℃ (room temperature)

C-V measurements are obtained by Boonton capacitance meter for noise determination and to find doping concentrations. Depletion capacitance dominates the reverse biased one, which is given as per Poisson's equation,

$$C_j = \frac{dQ}{dV} = \frac{dQ}{W_d \frac{dQ}{\varepsilon_s}} = \frac{\varepsilon_s}{W_d} \text{F/cm}^2 \qquad (2.13)$$

where Cj is the depletion capacitance, W_d is the depletion region, ε_s is the silicon permittivity, dV is the reverse bias voltage and dQ is the space charge.

Equation of depletion region is obtained by solving Poisson's formula as,

$$W_d = \sqrt{\frac{2\varepsilon_s(V_{bi}-V)}{qN_B}} \qquad (2.14)$$

where V_{bi} is the built in potential, q is the charge of an electron and N_b is the substrate doping concentration. When depletion width is plotted against reverse biased voltage, the following graph (figure 3) is obtained and the readings are tabulated (table 3).

Table 3.Voltage vs. depletion width

Voltage	Depletion width
1.20628	0.630689
2.98252	1.30732
4.27786	1.69139
5.41266	1.98541
6.63066	2.23478
8.82586	2.59845
10.1271	2.80316
12.5675	3.16737
15.0093	3.48675
17.3702	3.78352
19.5698	4.01267
23.3983	4.42484
25.6796	4.65417
29.3476	4.97631

From the graph plotted below, it is understood that the voltage level goes on increasing proportionally with depletion width.

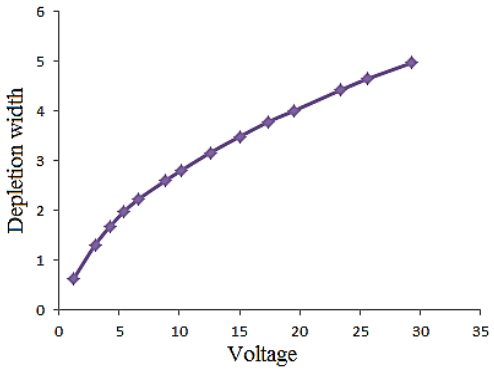

Figure 4.Voltage vs. depletion width

3.3. Construction

Microdosimeter device is packed with Lucite holder. The detector is connected to Canberra 2003T preamplifier in-turn to Canberra 2024 amplifier via 1m and 8m coaxial cable respectively. The output is the pulse voltage and the resultant from each digitized event is stored in multi-channel analyser.

Microdosimeter is encapsulated by an aluminium foil where it is fed to ground using a coaxial cable in-order to reduce noise signals. The output of the amplifier is proportional to energy deposition of the sensitive volume. Microdosimeter collects charge due to the passage of ion through its sensitive volume which depends upon the deposited energy since 3.6electron volt is required for the generation of an electron-hole pair in silicon.

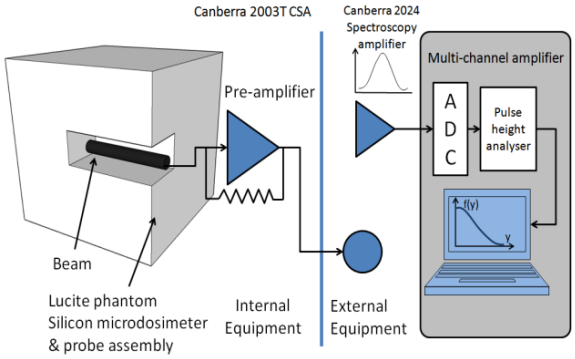

Figure 5.Construction of microdosimeter

Although noise minimisation is performed using aluminium foil, it is further minimised by enhancing protection (aluminium shield of relatively high thickness) from external electromagnetic field. It may also consist of non-conductive holes and gaps. Hence the construction is improved by using printed circuit board. The previous Canberra Charge Sensitive Amplifier (CSA) is replaced by AMPTEK A250. Microdosimeter of low noise circuit is shown in figure5.

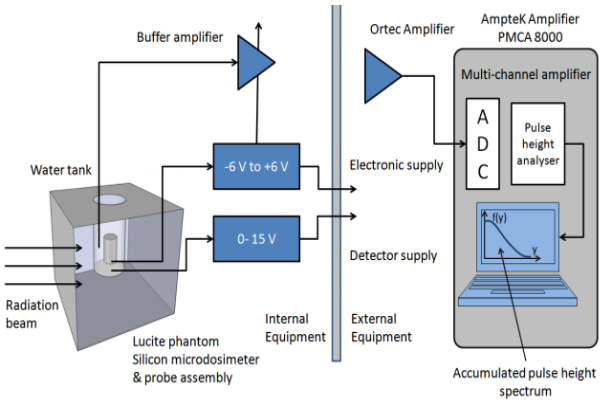

Figure 6.Microdosimeter of low noise circuit

In the above diagram (figure 6), JFET is employed as the input transistor along with a fast low noise buffer and a high speed operational amplifier. Characteristic impedance and proper termination are provided. To assist in low power supply, ceramic disc bypass capacitors are used. ±6V and (0-15) V supply are provided to power the probe meter and detector correspondingly. Lucite blocks are used to fill the air-gaps that occur between electronic meter and shield. Microdosimeter within printed circuit board is displayed below (figure 7) and its complete circuit diagram is given in figure B1.

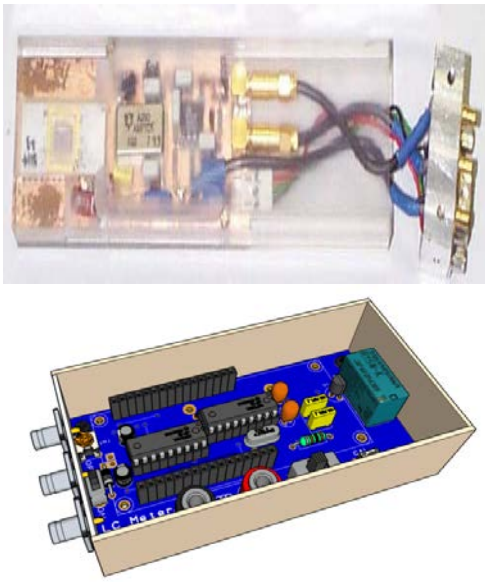

Figure 7.PCB mounted microdosimeter

3.4. Noise analysis

Thermal, shot and flicker are the basic noise factors to be considered in the design of the proposed dosimeter. Thermal noise arises out of thermal excitation and shot noise due to discrete dc biasing. Flicker noise is common in most of the circuits wherever there is a flow of direct current. JFET is used in this noise minimization model where thermal noise exceeds shot noise because of the majority carrier current flow. The channel resistance at which the transistor is located in active region is,

$$R_{ch} = \frac{1}{\gamma g_m} \qquad (2.15)$$

where g_m is the transconductance and γ is assumed to be 2/3. Thermal noise is expressed as,

$$\overline{\iota_{ch}^2} = {}^{4kT}/_{R_{ch}}\, df \qquad (2.16)$$

where k is the Boltzmann's constant and T= 300K. Thus the channel noise,

$$\overline{v_g^2} = \overline{\iota_{ch}^2}/g_m^2 \qquad (2.17)$$

When flicker noise gets added to this, the voltage noise at the gate input is given by,

$$v_{FET}^2 = \left(\frac{4kT\gamma}{g_m} + \frac{K_f}{C_g f}\right) df \qquad (2.18)$$

A noise model is constructed to optimize the noise performance. Considering all the primary noise sources, bias, feedback resistor thermal noise and detector current shot noise, the corresponding noise model for the proposed microdosimeter is shown below.

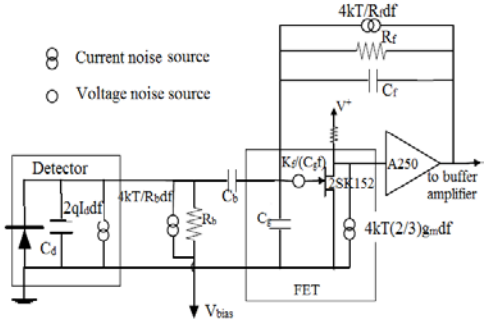

Figure 8.Noise model of microdosimeter

All the noise sources are referred to the amplifier output in-order to do noise determination and the total noise is defined by equivalent noise charge. Instruments such as detector input FET and preamplifier must be placed on a same integrated platform to enhance the noise performance. Silicon detectors of high resistivity might not be compatible and hence this work has been employed with the detector with lower depletion width which is readily compatible. This further simplifies the preamplifier and detector integration.

3.5. SOI design

Silicon-on-dosimeter consists of SOI diode arrays. Due to the shortcomings of first and second generation structures, the third generation model is proposed using planar process. Phosphorus and boron ions are implemented to create the p-i-n junction and a veto electrode is inserted to manage the charge collection. Its fabrication includes different materials of various shapes with appropriate spacing in-between. To have better signal to noise ratio by capacitance reduction, segmented technique is employed. Higher performance of the device is performed by providing minimal spacing between the cells in-turn in production of higher statistics. A schematic representation of single cell topology is given in figure 9.

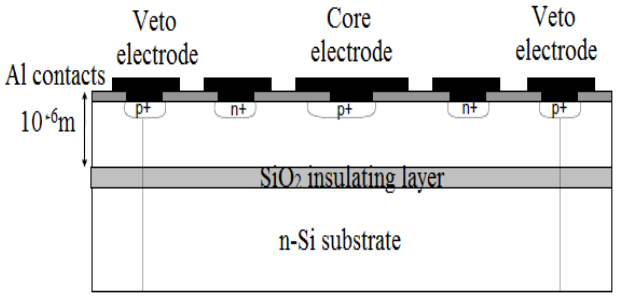

Figure 9.SOI microdosimeter device

3.6. TISSUE EQUIVALENCE

Tissue equivalence can be termed as muscle equivalence. Tissue substitutes are mixtures where their radiation interaction mechanism goes in hand with the tissue of the body. Even the atomic composition matches with body tissue as radiation properties do. The operational and construction requirements like mechanical structure, conductivity and stability do not come under tissue composition, rather, radiation and detector characteristics and mass densities are evaluated. Investigation on microdosimetric calculation to tissue volumes are rarely analysed in the existing methodologies. In-order to compare silicon and tissue, composition of tissue must be defined. All such biological components including muscle, skeleton, lung and adipose tissue, blood vessels, lymph, etc. are taken into consideration since they include under total body mass. Oxygen, carbon, hydrogen and nitrogen are the elements that build-up a tissue. Tissue quality varies with its composition, density matching, energy and type of the exposed radiation. The composition and the properties of some of the materials that could be compared to the tissue are listed in table A1. The elements added in the table are listed below.

- A150 is highly ductile which consists of carbon, polyethylene, calcium substitutes and nylon. This composition closely resembles that of muscle's hydrogen and nitrogen where the oxygen content is lower so that, it is increased to attain conductivity.
- Lucite is used as a tissue substitute which is included since it is simple, readily available and of low cost.

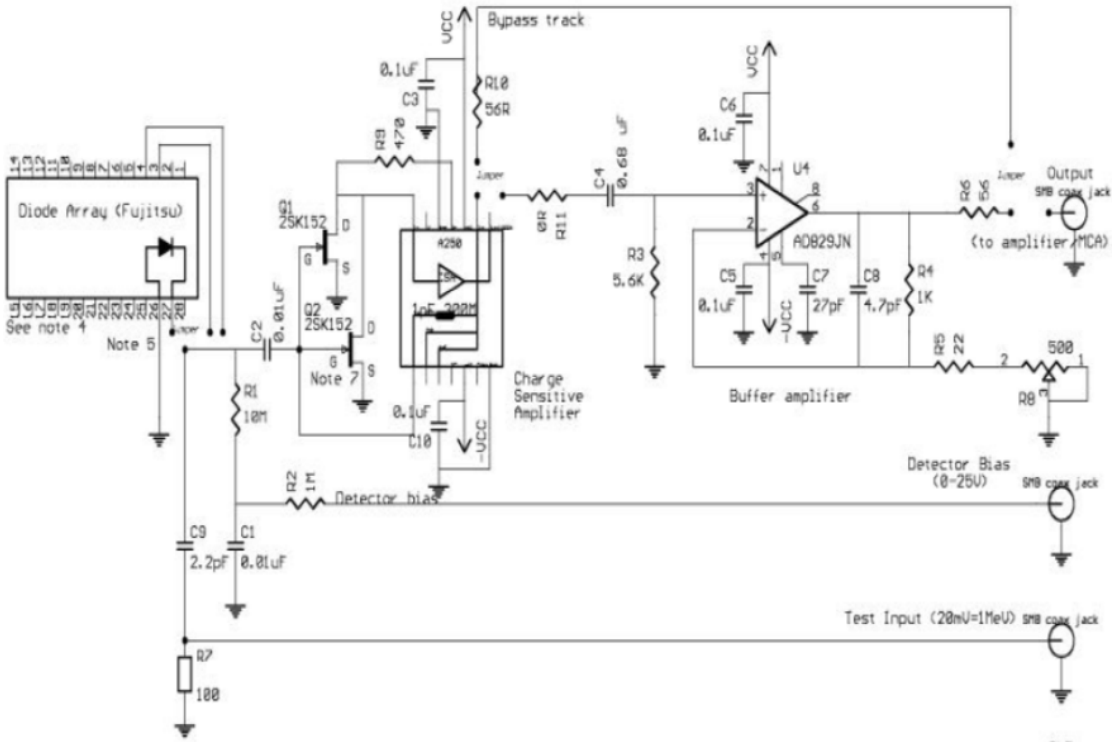

Figure B1.Circuit diagram of low noise prototype of microdosimeter

Table A1.Composition and properties of tissues and their substitutes

			Muscle		A150		Lucite		Silicon
Atom	**Z**	**A**	**Atomic %**	**Mass %**	**Atomic %**	**Mass %**	**Atomic% Mass%**	**Mass %**	**Mass &Atomic%**
H	1	1.01	63.31	10.2	58.26	10.1	53.33	8.05	0
C	6	12.01	6.41	12.3	37.61	77.7	33.33	59.98	0
N	7	14.01	1.56	3.5	1.45	3.5	0	0	0
O	8	16	28.51	72.91	1.89	5.2	13.33	31.96	0
F	9	19	0	0	0.52	1.7	0	0	0
Na	11	22.99	0.02	0.08	0	0	0	0	0
Si	14	28.09	0	0	0	0	0	0	100
P	15	30.97	0.04	0.2	0	0	0	0	0
Si	16	32.06	0.1	0.5	0	0	0	0	0
K	19	39.1	0.05	0.3	0	0	0	0	0
Ca	20	40.08	0.001	0.007	0.26	1.8	0	0	0
Mean Atomic Mass				14.1		11.8		12.4	28.09
Density(G/Cm^3)				1.04		1.127		1.2	2.32
Atomic Density*10^{23} Atoms/Cm^3				1		1.17		1.08	0.5
Electron Density*10^{23} Atoms/Cm^3				3.44		3.73		3.9	6.99

3.6.1. Correction factor

Linear energy transfer is the fundamental term to be analysed when concentrating on the performance of microdosimeter. Energy deposition varies with respect to the integral of the particles' transfer over the traverse of the chord length so that the prime factor in determining tissue equivalence is the consideration of range and energy of the particle other than LET and range. The range of a particle can be defined as,

$$R = \int_0^{E_{max}} \left(-\frac{dE}{dx}\right)^{-1} dE \qquad (2.19)$$

where E_{max} is the initial energy, dE/dx is the particle LET and R is the particle range.

dE/dx is given by,

$$-\frac{dE}{dx} = \frac{4\pi e^4 z^2}{m_0 v^2} NZ \left[\ln \frac{2m_0 v^2}{I} - \ln\left(1 - \frac{v^2}{c^2}\right) - \frac{v^2}{c^2}\right] \quad (6.2)$$

where v is the velocity of the particle, z is the particle charge, N is the number density, Z is the atomic number, m_0 is the electron rest mass, I is the average excitation and ionization and e is the charge of an electron.

To estimate the experimental parameter I, the following equation is considered.

$$\begin{cases} 19.0eV, Z = 1(hydrogen) \\ 11.2 + 11.7ZeV, 2 \le Z \le 13 \\ 52.8 + 8.71ZeV, Z > 13 \end{cases} \qquad (2.20)$$

The above equation could be opted for a simple material and for a mixture of material; individual constituents can be added

according to Bragg's additivity rule. Ziegler's Stopping and Ranges of Ions in Matter (Z-SRIM) program provides higher accuracy. Tissue substitute converter is employed and the particle range must be in a way that crossers and stoppers dominate in the microdosimetry.

To enable range comparison the expression could be,

$$\frac{R_2}{R_1} \cong \frac{\rho_1\sqrt{A_2}}{\rho_2\sqrt{A_1}} = \zeta \qquad (2.21)$$

where ρ and A are the density and atomic weight respectively, and ζ is the scaling factor.

For the rectangular parallelepiped tissue, the scaling factor can be ζx* ζy* ζz with a dimension x*y*z and for cylindrical and spherical structures, the scaling factor refers to linear dimension where the scaling factor of silicon detector corresponds to all ion units. Mean chord length should be same for both the tissue volume and the scaled silicon volume in-order to get equal tissue equivalence lineal energy. From the above equation, the scaling factor for A150, Lucite and silicon would be 0.84, 0.81 and 0.6 accordingly. The ratio of silicon interaction to converter interaction must be negligible so that the events begin from converter recoil units and not from silicon units. These are certain rules to be maintained by the silicon detector/tissue equivalence converter in obtaining tissue equivalence. Boron Neutron Capture Therapy (BNCT), Fast Neutron (FN) and Proton Therapy (PT) tissue equivalence are discussed and compared.

3.6.2. BNCT

To test the geometrical tissue equivalence factor, BNCT reactions are required. So the thermal neutron equation is expressed as,

$$^{14}_{7}N + {}^{1}_{0}n \rightarrow {}^{14}_{6}C + {}^{1}_{1}p \qquad (2.22)$$

$$^{10}_{5}B + {}^{1}_{0}n \xrightarrow{6.3\%} {}^{7}_{3}Li + {}^{4}_{2}He \qquad (2.23)$$

$$^{10}_{5}B + {}^{1}_{0}n \xrightarrow{93.7\%} {}^{7}_{3}Li + {}^{4}_{2}He + \gamma \qquad (2.24)$$

The ionic compounds and their energies are tabulated in table 4.

Table 4.Energy-range data

Reaction	Ion	Energy	Range (μm)	
			Tissue	Si
$^{14}N(n,p)^{14}C$	p	590	10.5	7.2
	^{14}C	40	0.2	0.12
$^{10}B(n,\alpha)^{7}Li$	α(6.3%)	1780	9.3	6.3
		1010	4.6	2.8
		1470	7.7	5.1
		840	4.1	2.5

The table calculations and data are based on SRIM coding and PRAL (Projected Range Algorithm) accordingly. To confirm whether the energy deposition in tissue resembles that of in silicon volumes, Monte Carlo program is developed. It is assumed that the ions travel in a straight line and that the volume is higher comparing to the width of the track assuming that the width is negligible. The above stated assumptions are valid if the energy of the ions is low and the volume is of micrometer in size. Generation and sensitive volumes are defined to analyse Monte Carlo program. The ion/energy readings in the above table yields average longitudinal range. In generation volume, ions are developed by appropriate nitrogen and boron concentration. By the generation of ion in generation volume, energy deposition is computed in terms of sensitive volume. The details of interaction data and ions are listed in table 5.

Table 5.Interaction data for BNCT

Reaction	σ	Inter-action	Ions	P
$^{14}N(n,p)^{14}C$	1.81	0.03	p, ^{14}C	0.4
$^{10}B(n,\alpha)^{7}Li$	3837	0.05	α, ^{7}Li(6.3%)	0.1
			α, ^{7}Li(93.7%)	0.6

An ionic pair is randomly selected based on the probability criteria as per table 4 and table 5. The position of the interaction and the angle of ion emission within the generation volumes are randomly selected. The degree of the ion pair emission is 180°. The points where the emitted ions intersect are calculated and the point that follows the ion path is selected. Though it is time consuming, it is adoptable for further versions.

3.6.3. Fast neutron and proton therapy

Fast neutron and proton therapy also takes tissue equivalence of silicon microdosimeter values from table 4. Some of the ionic outputs from fast neutron reactions are alphas, protons and heavy ion recoils. Normally, high energy protons dominate in the microdosimetric spectrum and so scaling factor should be of considerably low value. Tissue and silicon range ratio as in figure 10 assists in calculation of desired scaling factor of secondary recoil products. All the ions follow a usual shape with respect to Z. The curve of each ion moves to higher energy levels as Z moves forward.

Table 6.Tissue and silicon range for H, He, C and O

H	He	C	O
0.247678	0.366963	0.268733	0.301653
0.322515	0.328335	0.313632	0.325948
0.427112	0.337331	0.328721	0.349936
0.561648	0.257333	0.323029	0.323415
0.651525	0.266458	0.275582	0.293674
0.669694	0.302393	0.248949	0.296765
0.625471	0.350387	0.231311	0.231487
0.557242	0.610686	0.249511	0.249688
0.417594	0.649684	0.279481	0.237806
0.286765	0.655923	0.396154	0.264713
0.271949	0.614634	0.554774	0.336599
0.206494	0.510744	0.620921	0.432298
0.147117	0.388912	0.624305	0.555015
0.105747	0.266996	0.580133	0.615052
0.061475	0.204524	0.443528	0.600525
0.029295	0.207603	0.265139	0.493733
0.014752	0.071388	0.205682	0.148966

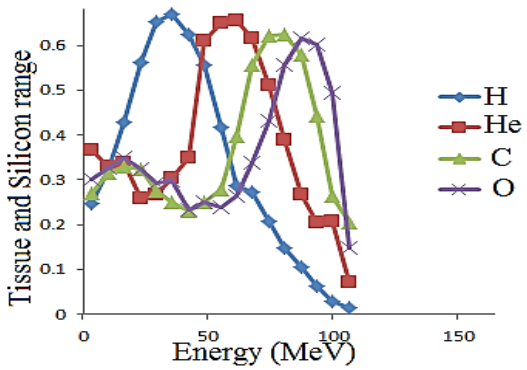

Figure 10.Tissue and silicon range for H, He, C&O

The range of tissue and silicon versus energy in MeV is plotted in the above graph shown in figure 10 from the values obtained from table 6. All the elemental curves differ among them by a slight

variation. The curves for hydrogen, helium, carbon and oxygen though begin and end in almost similar points, the attainment of their corresponding peak points vary.

3.7. Characterization of sensitive volume and radiation hardness

One of the common problems affecting silicon microdosimetry is poor characterization of sensitive volume. Since SOI structures are employed, diffusion and funnelling effects are reduced. The drawbacks of the existing system are overcome by precisely defining the charge collection modelling. Basic charge collection procedures are experimented as per physics. To construct sensitive volume and radiation hardness, the following strategies are used, namely alpha and proton micro-beam and alpha broad-beam spectroscopy along with 2D and 3D simulation.

- Broad-beam spectroscopy: It is the prime alpha spectroscopy where the beam area is wider than the microscopic area
- Micro-beam spectroscopy: It uses a scanned sub-micron diameter beam in which the charge collection data is directly provided. It also calculates the lifetime of minority carrier.

To analyse the suitability of devices employed under different fields, radiation hardness is determined where 2µm SOI and bulk apparatus are used. Furthermore, the funnelling effects are removed by the availability of proton beam in the micro-beam spectroscopy and the charge collection mechanism is effectively localised. Its results are highly accurate when radiation defects are minimised. After all, this method is quite expensive comparing to broad-beam spectroscopy. In case of simulation models, newer designs are evaluated faster with the use of 3D simulation but it is time consuming and 2D model is not accurate too.

4. Conclusion And Future Recommendations

Silicon dosimeter is designed with the aim of enhancing the sensitive surface area to yield sensitive volumes. Maximum accuracy is obtained by using Z-SRIM program. Key issues which influence the silicon microdosimetry including the diffusion and funnelling effects are significantly minimised due to the availability of SOI structures. Silicon based microdosimeter is designed accurately by defining boron neutron capture therapy, fast neutron and proton therapy tissue equivalence and by constructing sensitive volume and radiation hardness. Using detector with lower depletion width makes the SOI design more compatible and the microdosimetric calculations to tissue volumes becomes well organised. Silicon microdosimeter could have been developed by tissue cells using accurate muscle equivalent mixture. This procedure can be focussed on in future projects of designing silicon microdosimeter and again, sub-micron resolution of the micro-beam spectrum can be executed by reducing the radiation effects for a prolonged time period.

References

[1] P.D.Bradley, M.Zaider and A.B.Rosenfeld, Solid State Microdosimetry, Nuclear Instruments and Methods in Physics Research Section B: Beam Interactions with Materials and Atoms, Vol. 184, No. 1-2, 2001, pp. 135–157, http://dx.doi.org/10.1016/S0168-583X(01)00715-7.

[2] G.A.Santa Cruz, Microdosimetry: Principles and Applications, Reports of Practical Oncology & Radiotherapy, Vol. 21, No. 2, 2016, pp. 135-139.

[3] S.Agosteo, F.Dal Corso, A.Fazzi, F.Gonella, M.V.Introini, I.Lippi, M.Lorenzoli, M.Pegoraro, A.Pola, V.Varoli, and P.Zotto, The INFN Micro-Si Experiment: A Silicon Microdosimeter for Assessing Radiation Quality of Hadrontherapy Beams, AIP Conference Proceedings, Italy, 2013, http://dx.doi.org/10.1063/1.4812917.

[4] Anatoly B.Rosenfeld, Novel Detectors for Silicon Based Microdosimetry, their Concepts and Applications, Nuclear Instruments and Methods in Physics Research Section A: Accelerators, Spectrometers, Detectors and Associated Equipment, Vol. 809, 2016, pp. 156-170, http://dx.doi.org/10.1016/j.nima.2015.08.059.

[5] I.C.Cho, Wan H.Wen, T.C.Chao and Chuan-Jong Tung, Microdosimetry Measurements for Low-Energy Particles using a Mini TEPC with Removable Plug, Radiation Physics and Chemistry, 2016, http://dx.doi.org/10.1016/j.radphyschem.2016.01.030

[6] M.A.Xapsos, G.P.Summers, E.A.Bure and C.Poivey, Microdosimetry Theory for Microelectronics Applications, Nuclear Instruments and Methods in Physics Research Section B: Beam Interactions with Materials and Atoms, Vol. 184, No. 1-2, 2001, pp. 113–134, http://dx.doi.org/10.1016/S0168-583X(01)00716-9.

[7] C.Guardiola, A.Carabe, F.Gomez, G.Pellegrini, C.Fleta, S.Esteban, D.Quirion and M.Lozano, First Silicon Microdosimeters Based on Cylindrical Diodes, Sensors & Transducers, Vol. 183, No. 12, 2014, pp. 129-133 129.

[8] K.G.Kostov and Joaquim J.Barroso, Space-Charge-Limited Current in Cylindrical Diodes with Finite-Length Emitter, Physics of Plasmas, Vol. 9, No. 3, 2002, pp. 1039-1042, http://dx.doi.org/ 10.1063/1.1446876.

[9] T.Tran Linh, A.P.Dale, Guatelli Susanna, Petasecca Marco, L.F.Lerch Michael, R.Mark and R.Anatoly, 3D Bridge Microdosimeter: Charge Collection Study and Application to RBE Studies in 12C Radiation Therapy, Journal and Proceedings of the Royal Society of New South Wales, Vol. 148, No. 455/456, 2015.

[10] S.Agosteo, P.G.Fallica, A.Fazzi, A.Pola, G.Valvo and P.Zotto, A Feasibility Study of a Solid-State Microdosimeter, Applied Radiation and Isotopes, Vol. 63, No. 5-6, 2005, pp. 529-535, http://dx.doi.org/10.1016/j.apradiso.2005.05.001.

[11] D.Kathirvel and R.Jeyachitra, Structural Properties of Vacuum Evaporated ZnS Thin Films, International Journal of Macro and Nanophysics, Vol. 1, No. 1, 2016, pp. 57-69, http://dx.doi.org/10.18831/djphys.org/2016011006

[12] Ali Hussein Faraj Alnasraui, Impact of Stress and Radiation of Cellular Phones on Heart and its Functions, DJ International Journal of Advances in Electronics and Communication Engineering, Vol. 2, No. 2, 2016, pp. 1-10, http://dx.doi.org/10.18831/djece.org/2016021001